17th World Conference on Earthquake Engineering, 17WCEE
Sendai, Japan - September 13th to 18th 2020

IDENTIFICATION OF GEOMETRIC NONLINEARITY FORMULATIONS AND THE INFLUENCES ON STRUCTURAL DYNAMIC RESPONSES

K.K.F. Wong[1]

[1] *Research Structural Engineer, National Institute of Standards and Technology, USA, kfwong@nist.gov*

Abstract

Both ASCE/SEI 7-16 [1] and ASCE/SEI 41-17 [2] design standards require that *P*-Δ effects be included in the nonlinear dynamic analysis procedure for designing new and existing structures. However, software packages that perform nonlinear dynamic analysis typically only allow users to either 'turn on' or 'turn off' the effect of geometric nonlinearity without informing users what type of nonlinear effect is being included, such as whether both large *P*-Δ and small *P*-δ effects are included. Coupling this geometric nonlinearity effect with material nonlinearity of the structure can lead to significant differences in the predicted responses, especially when the structure is at near-collapse. Therefore, study on how geometric nonlinearity can affect structural performance is important to performance-based seismic engineering.

The challenge of how each software package handles the coupling between geometric and material nonlinearities often comes down to their interaction. The traditional method of structural analysis with material nonlinearity uses changing stiffness to quantify the stiffness reduction after yielding has occurred in the structure, which requires reformulation of the global stiffness matrix before solving for the displacement response. The difficulty comes in when the axial force reduces the stiffness of the member and at the same time when tangent stiffness is used after a nonlinear component has yielded. Will this axial force further reduce the tangent stiffness, and by how much? On the other hand, the use of tangent stiffness is typically derived based only on material nonlinearity with no consideration of geometric nonlinearity. At the same time, the use of geometric stiffness was derived based only on geometric nonlinearity with no consideration of material nonlinearity. Therefore, one needs to go back to the original derivation with the basic principles to answer this question.

In this paper, a detailed formulation of the nonlinear stiffness matrices taking into consideration both geometric and material nonlinearities is derived for a column member. It is followed by a study on how different software packages implement different geometric nonlinearity formulations and identify whether such formulation include both large *P*-Δ and small *P*-δ effects in the analysis. Finally, examples are presented to demonstrate how different formulations of geometric nonlinearity affect the nonlinear responses of framed structures.

Keywords: Geometric nonlinearity; Material nonlinearity; Large P-Δ effect; Small P-δ effect; Displacement

1. Introduction

Buildings constructed in seismic regions are vulnerable to strong ground shaking and thus are designed to sustain damage caused by material nonlinearity and remain stable by overcoming geometric nonlinearity. Nonlinear dynamic analysis with both geometric and material nonlinearities is currently the most accurate method of estimating the response to seismic events. For this reason, both ASCE/SEI 7-16 [1] and ASCE/SEI 41-17 [2] require that geometric nonlinearity be included in the nonlinear dynamic analysis procedure. However, software packages provide a geometric nonlinearity "button" but do not explicitly state the specific geometric nonlinearity formulation implemented in these packages. For example, some software packages may implement the full geometric stiffness formulation that includes both large *P*-Δ and small *P*-δ effects, while other software packages may implement the simpler *P*-Δ stiffness formulation that accounts for only *P*-Δ effect.

This research investigates how different software packages implement geometric nonlinearity affect the nonlinear dynamic response calculations. To accomplish this work, a detailed formulation of the nonlinear stiffness matrices taking into consideration both geometric and material nonlinearities is first derived for a column member. It is followed by a study on how different software packages implement different geometric nonlinearity formulations and identify whether such formulation include both large *P*-Δ and small *P*-δ effects in the analysis. Finally, examples are presented to demonstrate how different geometric nonlinearity formulations affect the nonlinear responses of framed structures.

2. Derivations of Stiffness Matrix with Both Geometric and Material Nonlinearities

The original beam theory with geometric nonlinearity [3-4] was first developed for elastic columns in the 1960's without consideration of any material nonlinearity. But its use is limited because of its complexity in the closed-form solution as compared to those formulations based on either the *P*-Δ stiffness approach [5] or the geometric stiffness approach [6]. However, to identify the geometric nonlinearity used in software packages, it is often important to go back to the fundamental principle and understand how each geometric nonlinearity formulation is developed. Therefore, the original theory that included geometric nonlinearity is rederived here and extended to include material nonlinearity. This is done by deriving the stiffness matrix for a column member with plastic hinges at both ends and subjected to a compressive force.

Four degrees of freedom (DOFs) and two plastic hinge locations (PHLs) are used to describe the movements at the two ends of a column member in a moment-resisting frame. These movements at the two ends include lateral displacement ($v(0)$ and $v(L)$), rotation ($v'(0)$ and $v'(L)$), and plastic rotations at the two plastic hinges (θ_a'' and θ_b''). To compute the member stiffness matrix $\mathbf{k}_i$, where i denotes the i^{th} member in the frame, each of these 4 DOFs and 2 PHLs is displaced independently by one unit as shown in Fig.1 while subjected to an axial compressive load *P*. Here, V_{1k}, M_{1k}, V_{2k}, and M_{2k} represent the required shear forces and moments at the two ends of the member to cause the deformation in the prescribed pattern, where $k = 1,\ldots,6$ represents the six cases of unit displacement patterns of the member's movements, and M_{ak} and M_{bk} represent the moment at plastic hinges '*a*' and '*b*', respectively, due to the prescribed pattern. Note that the '1' end coincides with plastic hinge '*a*' and the '2' end coincides with plastic hinge '*b*' in Fig.1.

Using the classical Bernoulli-Euler beam theory with homogeneous and isotropic material properties, where the moment is proportional to the curvature and plane sections are assumed to remain plane based on small displacements, the governing equilibrium equation describing the deflected shape of the member is

$$(EIv'')'' + Pv'' = 0 \tag{1}$$

where *E* is the elastic modulus, *I* is the moment of inertia, *v* is the lateral deflection, *P* is the axial compressive force on the member, and each prime represents taking derivatives of the corresponding variable with respect to the *x*-direction of the member. By assuming *EI* is constant along the member, the solution to the fourth-order ordinary differential equation given in Eq. (1) becomes:

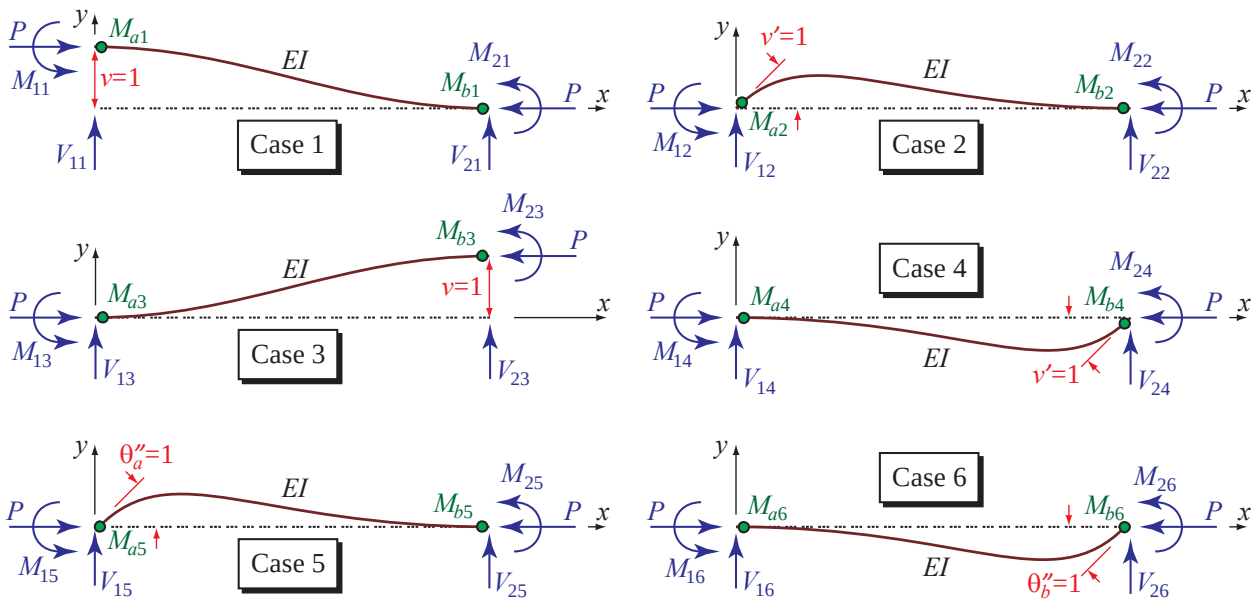

Fig. 1 – Six cases of unit displacement patterns and corresponding fixed-end forces and hinge moments

$$v = A\sin kx + B\cos kx + Cx + D \tag{2}$$

where $k^2 = P/EI$ and A, B, C, and D are constants to be determined by imposing different boundary conditions. Let $\lambda = kL$ to simplify the derivations, where L is the length of the member. The following cases of boundary conditions (starting with Case 4) are now considered.

2.1 Case 4

For Case 4 as shown in Fig.1, imposing the boundary conditions $v(0)=0$, $v'(0)=0$, $v(L)=0$, $v'(L)=1$, and $\theta''_a = \theta''_b = 0$ on Eq. (2) gives

$$v(0)=0: \qquad B + D = 0 \tag{3a}$$
$$v'(0)=0: \qquad kA + C = 0 \tag{3b}$$
$$v(L)=0: \qquad A\sin\lambda + B\cos\lambda + CL + D = 0 \tag{3c}$$
$$v'(L)=1: \qquad kA\cos\lambda - kB\sin\lambda + C = 1 \tag{3d}$$

Solving simultaneously for the constants in Eq. (3) gives

$$A = \frac{L(1-\cos\lambda)}{\lambda(\lambda\sin\lambda + 2\cos\lambda - 2)}, \quad B = \frac{L(\sin\lambda - \lambda)}{\lambda(\lambda\sin\lambda + 2\cos\lambda - 2)}, \quad C = -kA, \quad D = -B \tag{4}$$

Therefore, Eq. (2) along with the constants in Eq. (4) gives the deflected shape for Case 4. The shears (i.e., V_{14} and V_{24}) and moments (i.e., M_{14} and M_{24}) at the two ends of the member (see Fig.1) are then evaluated using the classical Bernoulli-Euler beam theory formula:

$$M(x) = EIv'' \quad , \quad V(x) = EIv''' + Pv' \tag{5}$$

Now taking derivatives of Eq. (2) and substituting the results into Eq. (5) while using the constants calculated in Eq. (4), the shears and moments at the two ends of the member are calculated as:

$$M_{14} = -EIv''(0) = EIk^2 B = \hat{s}\hat{c}EI/L \tag{6a}$$
$$V_{14} = EIv'''(0) + Pv'(0) = -EIk^3 A + P\times 0 = \bar{s}EI/L^2 \tag{6b}$$
$$M_{24} = EIv''(L) = -EIk^2(A\sin\lambda + B\cos\lambda) = \hat{s}EI/L \tag{6c}$$

$$V_{24} = -EIv'''(L) - Pv'(L) = EIk^3\left(A\cos\lambda - B\sin\lambda\right) - P\times 1 = -\bar{s}EI/L^2 \tag{6d}$$

where $\hat{s}$, $\hat{c}$, and $\bar{s}$ are the first three stability coefficients computed by the formula

$$\hat{s} = \frac{\lambda\left(\sin\lambda - \lambda\cos\lambda\right)}{2 - 2\cos\lambda - \lambda\sin\lambda} \quad , \quad \hat{c} = \frac{\lambda - \sin\lambda}{\sin\lambda - \lambda\cos\lambda} \quad , \quad \bar{s} = \hat{s} + \hat{s}\hat{c} = \frac{\lambda^2\left(1 - \cos\lambda\right)}{2 - 2\cos\lambda - \lambda\sin\lambda} \tag{7}$$

In addition, the moments at the two PHLs can be evaluated by recognizing that these moments must equal to the end moments by equilibrium, i.e., $M_{a4} = M_{14}$ and $M_{b4} = M_{24}$. Therefore,

$$M_{a4} = M_{14} = \hat{s}\hat{c}EI/L \quad , \quad M_{b4} = M_{24} = \hat{s}EI/L \tag{8}$$

2.2 Case 3

For Case 3 as shown in Fig.1, imposing the boundary conditions $v(0) = 0$, $v'(0) = 0$, $v(L) = 1$, $v'(L) = 0$, and $\theta_a'' = \theta_b'' = 0$ on Eq. (2) gives

$$v(0) = 0: \quad B + D = 0 \tag{9a}$$
$$v'(0) = 0: \quad kA + C = 0 \tag{9b}$$
$$v(L) = 1: \quad A\sin\lambda + B\cos\lambda + CL + D = 1 \tag{9c}$$
$$v'(L) = 0: \quad kA\cos\lambda - kB\sin\lambda + C = 0 \tag{9d}$$

Solving simultaneously for the constants in Eq. (9) gives

$$A = -\frac{\sin\lambda}{\lambda\sin\lambda + 2\cos\lambda - 2} \quad , \quad B = \frac{1 - \cos\lambda}{\lambda\sin\lambda + 2\cos\lambda - 2} \quad , \quad C = -kA \quad , \quad D = -B \tag{10}$$

These constants in Eq. (10) are used to give the deflected shape in Eq. (2) for Case 3. Now substituting Eq. (2) into Eq. (5) and using the constants calculated in Eq. (10), the shears and moments at the two ends of the member are calculated as:

$$M_{13} = -EIv''(0) = EIk^2B = -\bar{s}EI/L^2 \tag{11a}$$
$$V_{13} = EIv'''(0) + Pv'(0) = -EIk^3A + P\times 0 = -s'EI/L^3 \tag{11b}$$
$$M_{23} = EIv''(L) = -EIk^2\left(A\sin\lambda + B\cos\lambda\right) = -\bar{s}EI/L^2 \tag{11c}$$
$$V_{23} = -EIv'''(L) - Pv'(L) = EIk^3\left(A\cos\lambda - B\sin\lambda\right) - P\times 0 = s'EI/L^3 \tag{11d}$$

where s' is the fourth and final stability coefficient given by the formula

$$s' = 2\bar{s} - \lambda^2 = \frac{\lambda^3\sin\lambda}{2 - 2\cos\lambda - \lambda\sin\lambda} \tag{12}$$

In addition, the moments at the two PHLs are evaluated by equilibrium as

$$M_{a3} = M_{13} = -\bar{s}EI/L^2 \quad , \quad M_{b3} = M_{23} = -\bar{s}EI/L^2 \tag{13}$$

2.3 Case 2

For Case 2 as shown in Fig.1, by imposing the boundary conditions $v(0) = 0$, $v'(0) = 1$, $v(L) = 0$, $v'(L) = 0$, and $\theta_a'' = \theta_b'' = 0$ on Eq. (2), solution can be obtained via the same procedure presented above while solving for a different set of constants. On the other hand, a more direct solution can be obtained by recognizing that Case 2 is exactly the same as 'rotating' Case 4 by 180°. Doing so, the solution becomes

$$V_{12} = -V_{24} = \bar{s}EI/L^2 \quad , \quad V_{22} = -V_{14} = -\bar{s}EI/L^2 \tag{14a}$$
$$M_{12} = M_{24} = \hat{s}EI/L \quad , \quad M_{22} = M_{14} = \hat{s}\hat{c}EI/L \tag{14b}$$
$$M_{a2} = M_{b4} = \hat{s}EI/L \quad , \quad M_{b2} = M_{a4} = \hat{s}\hat{c}EI/L \tag{14c}$$

2.4 Case 1

For Case 1 as shown in Fig.1, by imposing the boundary conditions $v(0)=1$, $v'(0)=0$, $v(L)=0$, $v'(L)=0$, and $\theta''_a=\theta''_b=0$ on Eq. (2), solution can be obtained via the same procedure presented above while solving for a different set of constants. On the other hand, a more direct solution can be obtained by recognizing that Case 1 is exactly the same as 'flipping' Case 3 by 180°. Doing so, the solution becomes

$$V_{11}=V_{33}=s'EI/L^3 \quad , \quad V_{21}=V_{13}=-s'EI/L^3 \tag{15a}$$
$$M_{11}=-M_{23}=\bar{s}EI/L^2 \quad , \quad M_{21}=-M_{13}=\bar{s}EI/L^2 \tag{15b}$$
$$M_{a1}=-M_{b3}=\bar{s}EI/L^2 \quad , \quad M_{b1}=-M_{a3}=\bar{s}EI/L^2 \tag{15c}$$

2.5 Case 5

For Case 5 as shown in Fig.1, by imposing the boundary conditions $\theta''_a=1$, $\theta''_b=0$, and $v(0)=v'(0)=v(L)=v'(L)=0$ on Eq. (2), solution can be obtained via direct comparison of Case 2 and Case 5, where a unit plastic rotation at hinge '*a*' gives the same displacement pattern as a unit rotation at the '1' end. It follows that the forces and moments at the four DOFs and two PHLs are the same for both cases, i.e.,

$$V_{1a}=V_{12}=\bar{s}EI/L^2 \quad , \quad V_{2a}=V_{22}=-\bar{s}EI/L^2 \tag{16a}$$
$$M_{1a}=M_{12}=\hat{s}EI/L \quad , \quad M_{2a}=M_{22}=\hat{s}\hat{c}EI/L \tag{16b}$$
$$M_{aa}=M_{a2}=\hat{s}EI/L \quad , \quad M_{ba}=M_{b2}=\hat{s}\hat{c}EI/L \tag{16c}$$

2.6 Case 6

Finally, for Case 6 as shown in Fig.1, by imposing the boundary conditions $\theta''_a=0$, $\theta''_b=1$, and $v(0)=v'(0)=v(L)=v'(L)=0$ on Eq. (2), solution can be obtained via direct comparison of Case 4 and Case 6, where a unit plastic rotation at hinge '*b*' gives the same displacement pattern as a unit rotation at the '2' end. It follows that the forces and moments at the four DOFs and two PHLs are the same for both cases, i.e.,

$$V_{1b}=V_{14}=\bar{s}EI/L^2 \quad , \quad V_{2b}=V_{24}=-\bar{s}EI/L^2 \tag{17a}$$
$$M_{1b}=M_{14}=\hat{s}\hat{c}EI/L \quad , \quad M_{2b}=M_{24}=\hat{s}EI/L \tag{17b}$$
$$M_{ab}=M_{a4}=\hat{s}\hat{c}EI/L \quad , \quad M_{bb}=M_{b4}=\hat{s}EI/L \tag{17c}$$

2.7 Stiffness Matrices

In summary, based on Eqs. (6), (8), (11), (13), and (14)-(17) for the above six cases, the small-displacement-based stiffness matrix of the i^{th} member $\mathbf{k}_i^{SF}$ for bending while considering both geometric and material nonlinearities becomes

$$\mathbf{k}_i^{SF}=\frac{EI}{L^3}\left[\begin{array}{cccc:cc} s' & \bar{s}L & -s' & \bar{s}L & \bar{s}L & \bar{s}L \\ \bar{s}L & \hat{s}L^2 & -\bar{s}L & \hat{s}\hat{c}L^2 & \hat{s}L^2 & \hat{s}\hat{c}L^2 \\ -s' & -\bar{s}L & s' & -\bar{s}L & -\bar{s}L & -\bar{s}L \\ \bar{s}L & \hat{s}\hat{c}L^2 & -\bar{s}L & \hat{s}L^2 & \hat{s}\hat{c}L^2 & \hat{s}L^2 \\ \hdashline \bar{s}L & \hat{s}L^2 & -\bar{s}L & \hat{s}\hat{c}L^2 & \hat{s}L^2 & \hat{s}\hat{c}L^2 \\ \bar{s}L & \hat{s}\hat{c}L^2 & -\bar{s}L & \hat{s}L^2 & \hat{s}\hat{c}L^2 & \hat{s}L^2 \end{array}\right] \begin{array}{l} \leftarrow v(0) \\ \leftarrow v'(0) \\ \leftarrow v(L) \\ \leftarrow v'(L) \\ \leftarrow \theta''_a \\ \leftarrow \theta''_b \end{array} \tag{18}$$

where the superscript '*SF*' denotes the member stiffness matrix $\mathbf{k}_i$ is formulated by using the stability functions method that is computed based on the stability coefficients in Eqs. (7) and (12). Note again that $\mathbf{k}_i$ is 6×6, where the 6 movements are associated with the displacements and rotations at the two ends (i.e., 4 DOFs) and the plastic rotations at the two plastic hinge locations (i.e., 2 PHLs).

Linearization of Eq. (18) can be performed by using Taylor series expansion on each term of the member stiffness matrix and truncating higher-order terms. Doing so gives

$$\mathbf{k}_i^{GS} = \frac{EI}{L^3}\begin{bmatrix} 12 & 6L & -12 & 6L \\ 6L & 4L^2 & -6L & 2L^2 \\ -12 & -6L & 12 & -6L \\ 6L & 2L^2 & -6L & 4L^2 \end{bmatrix} - \begin{bmatrix} 6P/5L & P/10 & -6P/5L & P/10 \\ P/10 & 2PL/15 & -P/10 & -PL/30 \\ -6P/5L & -P/10 & 6P/5L & -P/10 \\ P/10 & -PL/30 & -P/10 & 2PL/15 \end{bmatrix} \begin{matrix} \leftarrow v(0) \\ \leftarrow v'(0) \\ \leftarrow v(L) \\ \leftarrow v'(L) \end{matrix} \tag{19}$$

where the first matrix in Eq. (19) represents that classic stiffness matrix without considering any geometric nonlinearity, and the second matrix represents the geometric stiffness. The superscript '*GS*' denotes the member stiffness matrix $\mathbf{k}_i$ is formulated by using the geometric stiffness method. Note that the member stiffness matrix in Eq. (19) is a 4×4 matrix, where the rows and columns associated with θ_a'' and θ_b'' are dropped. This is because solution algorithms among various software packages that incorporate geometric nonlinearity using the geometric stiffness method usually adopt a different and independent algorithm for material nonlinearity.

Finally, the member stiffness matrix $\mathbf{k}_i$ in Eq. (19) can be further simplified by retaining only the large *P*-Δ effect while ignoring small *P*-δ effect. This is done by removing all geometric nonlinear terms associated with bending. Doing so gives

$$\mathbf{k}_i^{PD} = \frac{EI}{L^3}\begin{bmatrix} 12 & 6L & -12 & 6L \\ 6L & 4L^2 & -6L & 2L^2 \\ -12 & -6L & 12 & -6L \\ 6L & 2L^2 & -6L & 4L^2 \end{bmatrix} - \begin{bmatrix} P/L & 0 & -P/L & 0 \\ 0 & 0 & 0 & 0 \\ -P/L & 0 & P/L & 0 \\ 0 & 0 & 0 & 0 \end{bmatrix} \begin{matrix} \leftarrow v(0) \\ \leftarrow v'(0) \\ \leftarrow v(L) \\ \leftarrow v'(L) \end{matrix} \tag{20}$$

where the superscript '*PD*' denotes the member stiffness matrix $\mathbf{k}_i$ is formulated by using the *P*-Δ stiffness method.

3. Identification of Geometric Nonlinearity Using a Single Degree of Freedom System

An appropriate model should be used to serve the purpose of the study. To identify the geometric nonlinearity used in different software packages, consider the single degree of freedom (SDOF) column model as shown in Fig.2a be subjected to a constant axial compressive force *P*. Let the mass be *M*, damping be *C*, elastic modulus be *E*, moment of inertia be *I*, and length be *L*. The degree of freedom is set up so that the mass is restrained from rotation, but it is free to translate in the horizontal direction.

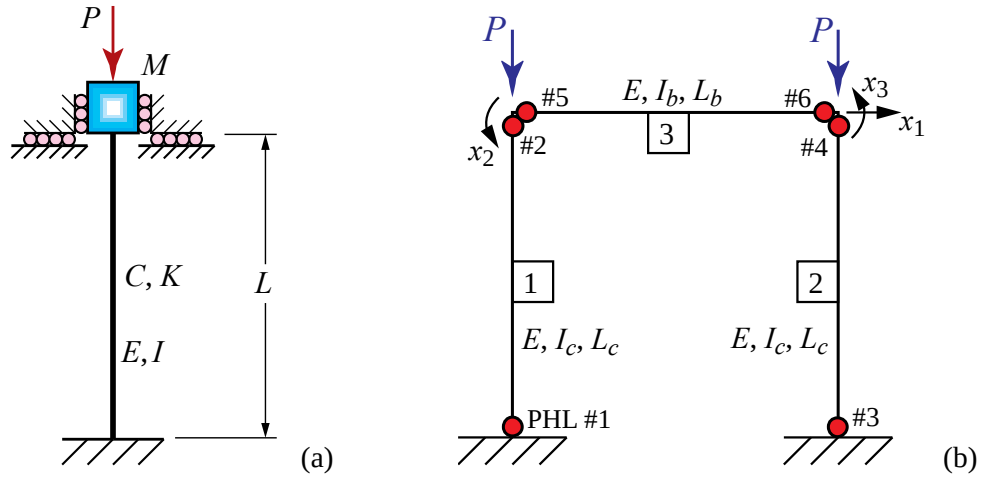

Fig. 2 – Single degree of freedom models with geometric nonlinearity

Based on this set up, the column experiences a constant axial force due to the gravity load only and also experiences shear and moment due to the earthquake ground motion only. Therefore, the lateral stiffness

of the column remains constant with a constant axial force throughout the entire earthquake time history analysis. If geometric nonlinearity is totally ignored in this problem, the lateral stiffness related to the horizontal translation degree of freedom at the top of the column is simply:

$$K_{OR} = \frac{12EI}{L^3} \tag{21}$$

where K_{OR} represents the original stiffness of the SDOF system without considering any geometric nonlinearity. If geometric nonlinearity is considered using the *P*-Δ stiffness approach, the lateral stiffness of the SDOF column (see Eq. (20)) becomes:

$$K_{P\Delta} = \frac{12EI}{L^3} - \frac{P}{L} \tag{22}$$

where $K_{P\Delta}$ denotes the geometrically nonlinear stiffness of the column using the *P*-Δ approach (i.e., including large *P*-Δ effect but excluding small *P*-δ effect). If geometric nonlinearity is considered using the geometric stiffness approach, the lateral stiffness of the SDOF column (see Eq. (19)) becomes:

$$K_{GS} = \frac{12EI}{L^3} - \frac{6P}{5L} \tag{23}$$

where K_{GS} denotes the geometrically nonlinear stiffness of the column using the geometric stiffness approach (i.e., including both large *P*-Δ and small *P*-δ effects). Finally, if geometric nonlinearity is considered through the use of stability functions, the stiffness matrix (see Eq. (18)) becomes:

$$K_{SF} = \frac{s'EI}{L^3} \tag{24}$$

where K_{SF} denotes the geometrically nonlinear stiffness computed using the stability functions approach (i.e., including both large *P*-Δ and small *P*-δ effects in a consistent form), and s' is the stability coefficients defined in Eq. (12).

In this study, let $E = 100$ GPa, $I = 6.4\times10^5$ mm^4, $L = 4$ m, and $P = 4$ kN in compression. Using a mass of $M = 9500$ kg, the calculated stiffnesses and the corresponding periods of vibration are summarized in Table 1. Note that the critical buckling load for the SDOF column is $P_{cr} = \pi^2 EI/L^2 = 39.48$ kN, which means the applied load is at 10.1 % of the critical buckling load (i.e., $P/P_{cr} = 0.101$). At this axial compressive force level, it is observed that $K_{GS} \approx K_{SF}$, but there is a 1.9 % difference in stiffness between $K_{P\Delta}$ and K_{GS} . This suggests that ignoring small *P*-δ effect can result in an increase in lateral stiffness by 1.9 %. Table 1 also shows that the difference between using $K_{P\Delta}$ and using K_{GS} results in a 1.0 % difference in the calculated period of vibration of the SDOF column. Note that 1.0 % elongation of period is sufficient to provide the phase shift needed to identify the geometric nonlinearity used in software packages.

Table 1 – Comparison of geometric nonlinear stiffnesses, periods, and maximum responses

	Stiffness (kN/m)	Period (s)	Max Displacement (m)	Max Velocity (m/s)	Max Acceleration (g)
K_{OR}	12.0	1.496	0.6990	2.996	1.258
$K_{P\Delta}$	11.0	1.562	0.6737	2.789	1.111
K_{GS}	10.8	1.577	0.6625	2.746	1.073
K_{SF}	10.799	1.577	0.6624	2.746	1.073

By assuming 0 % damping, the SDOF column shown in Fig.2a is now subjected to the 1995 Kobe earthquake as shown in Fig.3. The resulting displacement responses using the original stiffness (OR), *P*-Δ stiffness (PD), geometric stiffness (GS), and stability function stiffness (SF) are presented in Fig.4. In

addition, the maximum displacement, velocity, and absolute acceleration for using various geometric nonlinear stiffness approaches are summarized in Table 1. It can be seen from Fig. 4 that the responses using K_{GS} match those using K_{SF} well at such a small axial compressive force. The differences are more noticeable between the responses using $K_{P\Delta}$ and those using K_{GS}, where the maximum displacement response using $K_{P\Delta}$ increases by 1.7 % and the maximum acceleration response also increases by 3.5 %.

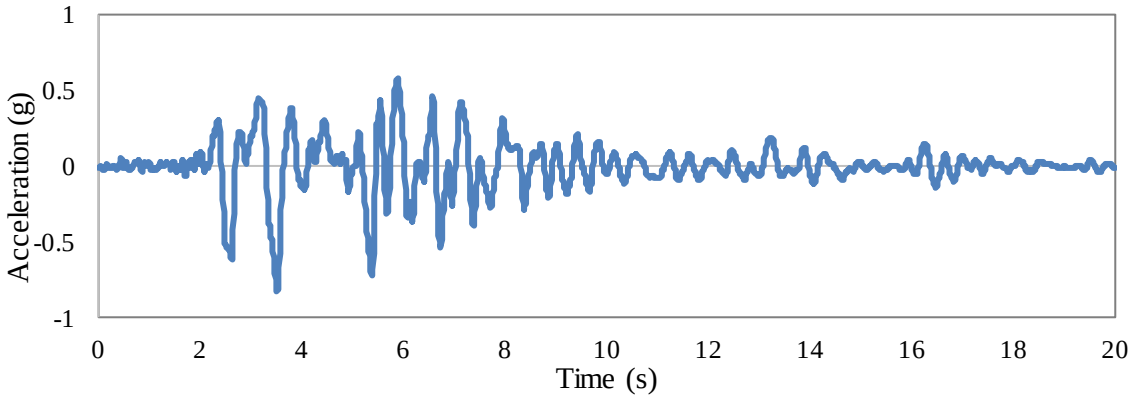

Fig. 3 – 1995 Kobe earthquake ground acceleration time history

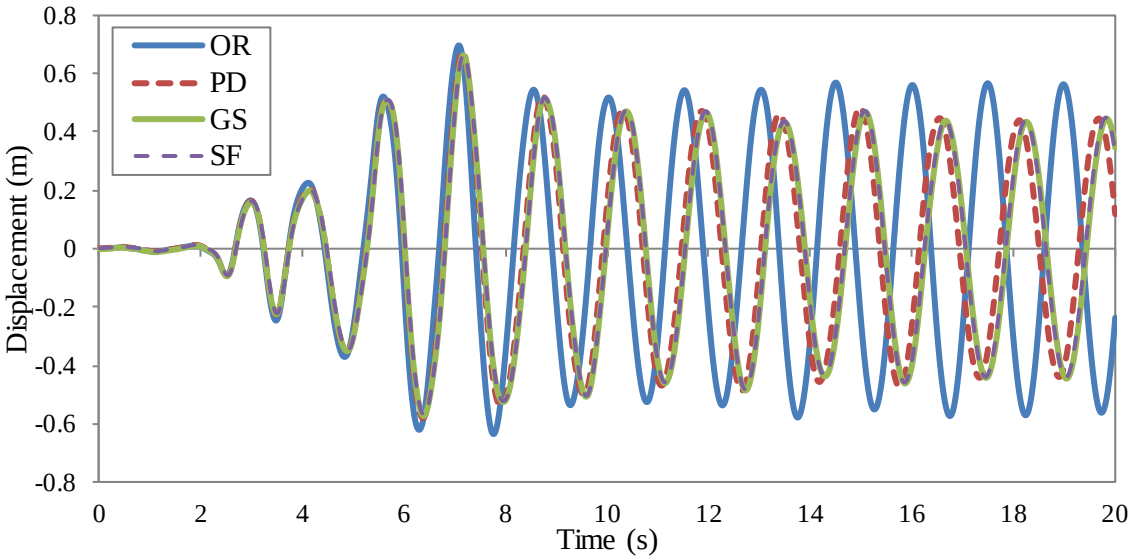

Fig. 4 – Displacement responses of the SDOF column using different stiffnesses

Knowing the stiffness of the column is important because it can be used to assess the type of geometric nonlinearity that is embedded in various software packages. Consider the same SDOF column shown in Fig.2a is now modeled using four small-displacement-based software packages commonly used in the United States, randomly labeled as S1, S2, S3, and S4, and is subjected to the 1995 Kobe earthquake shown in Fig.3. By assuming 0 % damping, Fig.5 shows the displacement responses from these software packages, and these responses are compared with those in Fig.4. As shown in Fig.5a, the comparison shows an exact match between the current analysis method using K_{GS} and the software packages S1 and S4. Similarly, Fig.5b shows an exact match between the current analysis method with $K_{P\Delta}$ and software packages S2 and S3. This indicates two of the small-displacement software packages use geometric stiffness that considers both large P-Δ and small P-δ effects in the formulation, while the other two of the small-displacement software packages use P-Δ stiffness that considers only large P-Δ effects and ignores the small P-δ effects. Note that even though using 0 % damping is an idealized situation, it helps eliminate the potentially differing effects of using damping parameters on the responses that may occur due to differences in damping formulations used in different software packages.

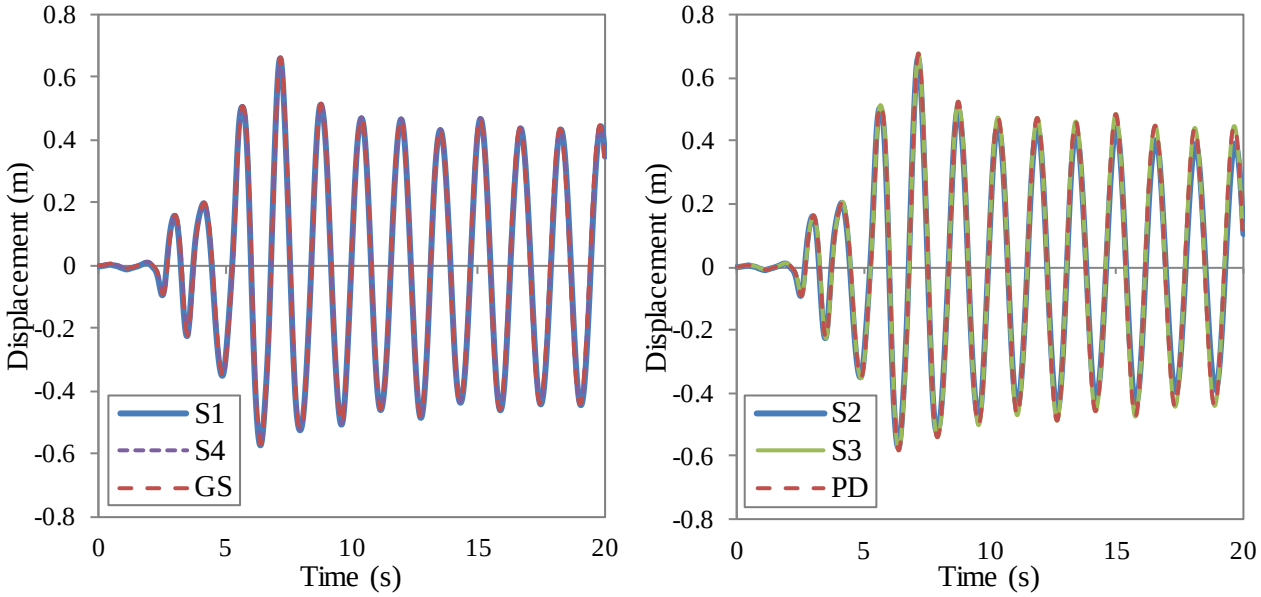

Fig. 5 – Displacement response comparisons between various software packages and manual calculations

4. One-Story Moment Frame

Once the type of geometric nonlinearity is known, the influence of using different types of geometric nonlinearity on displacement responses can be assessed. As a simple numerical example, consider a one-story one-bay moment-resisting frame as shown in Fig.2b with members assumed to be axially rigid. This gives a total of 3 DOFs (i.e., $n=3$) and 6 PHLs (i.e., $m=6$) as shown in the figure. Software packages S1 (based on GS) and S2 (based on PD) are selected for this study along with the SF method. Since using SF formulation is an uncommon approach with limited documentations, it is therefore worthwhile to discuss the analysis approach here. Based on Eq. (18), the member stiffness matrix for the two columns can be written as:

$$\mathbf{k}_i = \frac{EI_c}{L_c^3}\left[\begin{array}{cccc|cc} s_i' & \bar{s}_i L_c & -s_i' & \bar{s}_i L_c & \bar{s}_i L_c & \bar{s}_i L_c \\ \bar{s}_i L_c & \hat{s}_i L_c^2 & -\bar{s}_i L_c & \hat{s}_i \hat{c}_i L_c^2 & \hat{s}_i L_c^2 & \hat{s}_i \hat{c}_i L_c^2 \\ -s_i' & -\bar{s}_i L_c & s_i' & -\bar{s}_i L_c & -\bar{s}_i L_c & -\bar{s}_i L_c \\ \bar{s}_i L_c & \hat{s}_i \hat{c}_i L_c^2 & -\bar{s}_i L_c & \hat{s}_i L_c^2 & \hat{s}_i \hat{c}_i L_c^2 & \hat{s}_i L_c^2 \\ \hline \bar{s}_i L_c & \hat{s}_i L_c^2 & -\bar{s}_i L_c & \hat{s}_i \hat{c}_i L_c^2 & \hat{s}_i L_c^2 & \hat{s}_i \hat{c}_i L_c^2 \\ \bar{s}_i L_c & \hat{s}_i \hat{c}_i L_c^2 & -\bar{s}_i L_c & \hat{s}_i L_c^2 & \hat{s}_i \hat{c}_i L_c^2 & \hat{s}_i L_c^2 \end{array}\right], \quad i=1,2 \tag{25}$$

where $\hat{s}_i$, $\hat{c}_i$, $\bar{s}_i$, and s_i' are stability coefficients of the i^{th} column member computed using Eqs. (7) and (12). No axial force is acting on the beam member, and therefore the beam member stiffness matrix becomes:

$$\mathbf{k}_3 = \frac{EI_b}{L_b^3}\left[\begin{array}{cccc|cc} 12 & 6L_b & -12 & 6L_b & 6L_b & 6L_b \\ 6L_b & 4L_b^2 & -6L_b & 2L_b^2 & 4L_b^2 & 2L_b^2 \\ -12 & -6L_b & 12 & -6L_b & -6L_b & -6L_b \\ 6L_b & 2L_b^2 & -6L_b & 4L_b^2 & 2L_b^2 & 4L_b^2 \\ \hline 6L_b & 4L_b^2 & -6L_b & 2L_b^2 & 4L_b^2 & 2L_b^2 \\ 6L_b & 2L_b^2 & -6L_b & 4L_b^2 & 2L_b^2 & 4L_b^2 \end{array}\right] \tag{26}$$

Assembling the above member stiffness matrices into the global stiffness matrix gives a 9×9 stiffness matrix, which can be partitioned into the form

$$\mathbf{K}^{SF} = \left[\begin{array}{c|c} \mathbf{K}_{n\times n} & \mathbf{K}'_{n\times m} \\ \hline \mathbf{K}'^{T}_{m\times n} & \mathbf{K}''_{m\times m} \end{array}\right] = \left[\begin{array}{c|c} \mathbf{K}_{3\times 3} & \mathbf{K}'_{3\times 6} \\ \hline \mathbf{K}'^{T}_{6\times 3} & \mathbf{K}''_{6\times 6} \end{array}\right] \begin{array}{l} \leftarrow x_1, x_2, x_3 \\ \leftarrow \theta''_1, \ldots, \theta''_6 \end{array} \tag{27}$$

where

$$\mathbf{K}_{3\times 3} = \begin{bmatrix} (s'_1 + s'_2)EI_c/L_c^3 & \bar{s}_1 EI_c/L_c^2 & \bar{s}_2 EI_c/L_c^2 \\ \bar{s}_1 EI_c/L_c^2 & \hat{s}_1 EI_c/L_c + 4EI_b/L_b & 2EI_b/L_b \\ \bar{s}_2 EI_c/L_c^2 & 2EI_b/L_b & \hat{s}_2 EI_c/L_c + 4EI_b/L_b \end{bmatrix} \begin{array}{l} \leftarrow x_1 \\ \leftarrow x_2 \\ \leftarrow x_3 \end{array} \tag{28a}$$

$$\mathbf{K}'_{3\times 6} = \left[\begin{array}{cc|cc|cc} \bar{s}_1 EI_c/L_c^2 & \bar{s}_1 EI/L_c^2 & \bar{s}_2 EI_c/L_c^2 & \bar{s}_2 EI_c/L_c^2 & 0 & 0 \\ \hat{s}_1\hat{c}_1 EI_c/L_c & \hat{s}_1 EI_c/L_c & 0 & 0 & 4EI_b/L_b & 2EI_b/L_b \\ 0 & 0 & \hat{s}_2\hat{c}_2 EI_c/L_c & \hat{s}_2 EI_c/L_c & 2EI_b/L_b & 4EI_b/L_b \end{array}\right] \begin{array}{l} \leftarrow x_1 \\ \leftarrow x_2 \\ \leftarrow x_3 \end{array} \tag{28b}$$

$$\mathbf{K}''_{6\times 6} = \left[\begin{array}{cc|cc|cc} \hat{s}_1 EI_c/L_c & \hat{s}_1\hat{c}_1 EI_c/L_c & 0 & 0 & 0 & 0 \\ \hat{s}_1\hat{c}_1 EI_c/L_c & \hat{s}_1 EI_c/L_c & 0 & 0 & 0 & 0 \\ \hline 0 & 0 & \hat{s}_2 EI_c/L_c & \hat{s}_2\hat{c}_2 EI_c/L_c & 0 & 0 \\ 0 & 0 & \hat{s}_2\hat{c}_2 EI_c/L_c & \hat{s}_2 EI_c/L_c & 0 & 0 \\ \hline 0 & 0 & 0 & 0 & 4EI_b/L_b & 2EI_b/L_b \\ 0 & 0 & 0 & 0 & 2EI_b/L_b & 4EI_b/L_b \end{array}\right] \begin{array}{l} \leftarrow \theta''_1 \\ \leftarrow \theta''_2 \\ \leftarrow \theta''_3 \\ \leftarrow \theta''_4 \\ \leftarrow \theta''_5 \\ \leftarrow \theta''_6 \end{array} \tag{28c}$$

Assume that the frame shown in Fig.2b has a mass of 318.7 Mg and a damping of 0 %. Also, let $E = 200$ GPa, $I_b = I_c = 4.995\times10^8$ mm^4, $L_b = 7.62$ m, $L_c = 4.57$ m, and $P = 5{,}338$ kN. To include material nonlinearity in the analysis, assume that all six plastic hinges exhibit elastic-plastic behavior with plastic moment capacities of $m_b = 3130$ kN·m for the beam and $m_c = 3909$ kN·m for the two columns. By subjecting the frame to the 1995 Kobe earthquake ground motion as shown in Fig.3 with a scale factor of 1.3, the global displacement response at DOF #1 (i.e., roof displacement) is plotted in Fig.6 based on the stiffness matrices using stability function formulations (SF) in Eq. (28). In addition, the same undamped responses obtained from the software package S1 that uses geometric stiffness (GS) and the software package S2 that uses *P*-Δ stiffness (PD) are plotted in the figure for comparison. It is observed that the choice of geometric nonlinearity used in the analysis can influence the response calculations even for a simple SDOF system. While the responses calculated using SF and GS are reasonably close to each other, the calculated response using PD is quite different from the other two calculated responses.

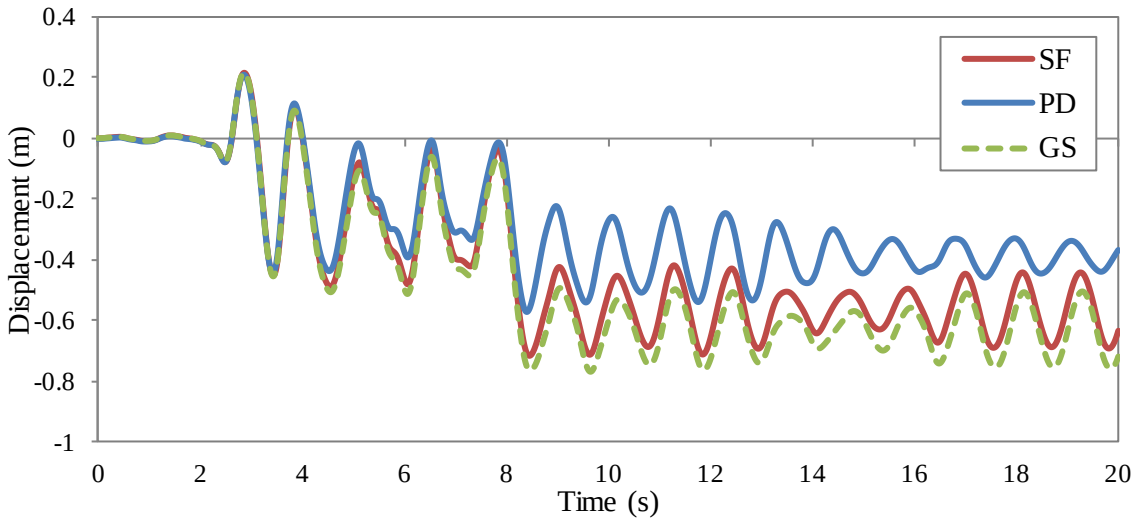

Fig. 6 – Displacement response comparisons of a one-story frame with various geometric nonlinearities

5. Four-Story Moment-Resisting Frame

Consider the four-story moment-resisting steel frame as shown in Fig.7a. This frame contains 36 DOFs (i.e., $n = 36$) and 56 PHLs (i.e., $m = 56$). Assume a mass of 72 670 kg is used on each floor, and no mass or mass moment of inertia is assigned to any of the vertical translation DOFs nor rotation DOFs. A gravity load of 863 kN is applied on each exterior column member and 1263 kN is applied on each interior column member as shown in Fig.7b. In addition, 0 % damping is assumed in order to provide a better comparison of the response among different software packages, including software package S2 that uses P-Δ stiffness (PD) and LS-DYNA finite element software package (LD) that uses large displacement formulation. For stability function (SF), the global stiffness matrix in Eq. (27) after assembly includes $\mathbf{K}_{36\times36}$, $\mathbf{K}'_{36\times56}$, and $\mathbf{K}''_{56\times56}$.

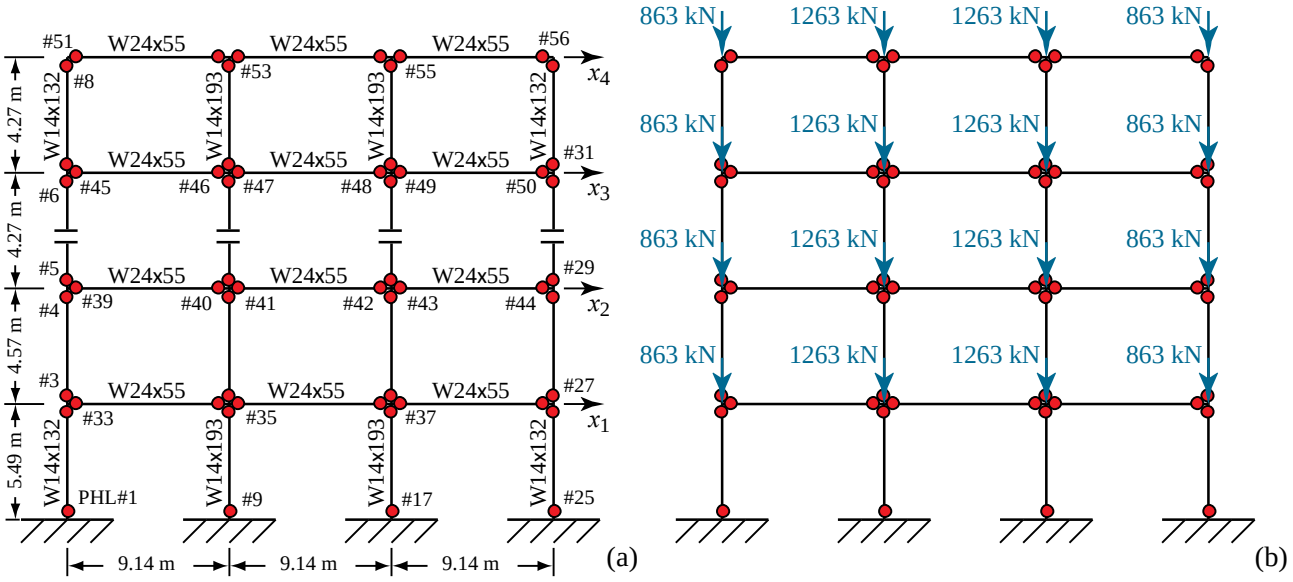

Fig. 7 – Four-story moment-resisting steel frame with gravity loads

Assume the yield stress of the member is 345 MPa and all 56 plastic hinges exhibit elastic-plastic behavior. The steel frame is now subjected to the 1995 Kobe earthquake ground motion as shown in Fig.3 with scale factors of 0.6, 0.8, 1.0, and 1.2. The roof displacement responses are summarized in Fig.8. Based on the results, it is observed that the responses computed using different geometric nonlinearity are similar at a scale factor of 0.6 when the response is only slightly nonlinear. However, the PD response begins to deviate at a scale factor of 0.8 with significant differences at a scale factor of 1.0. This suggests that using PD software packages that captures only large P-Δ effect while ignoring small P-δ effects may not be appropriate for computation when the significant coupling between geometric nonlinearity and material nonlinearity is expected.

6. Conclusion

In this paper, different formulations of geometric nonlinearity were presented with a detailed derivation of the stability functions stiffness matrix while incorporating material nonlinearity. Through this derivation, how each formulation captures large P-Δ and small P-δ effects were explained, and the investigation continued with a study on how different software packages implement geometric nonlinearity. A SDOF column was modeled using four different small-displacement-based software packages. Based on the output dynamic responses it was identified that two packages use P-Δ stiffness that includes only large P-Δ effects while the other two packages use geometric stiffness that includes both large P-Δ and small P-δ effects. The study was then extended to see how different formulations of geometric nonlinearity impact the response of moment-resisting frame, and it was shown that software packages implementing P-Δ stiffness can lead to different calculated results when there is significant coupling between geometric and material nonlinearities.

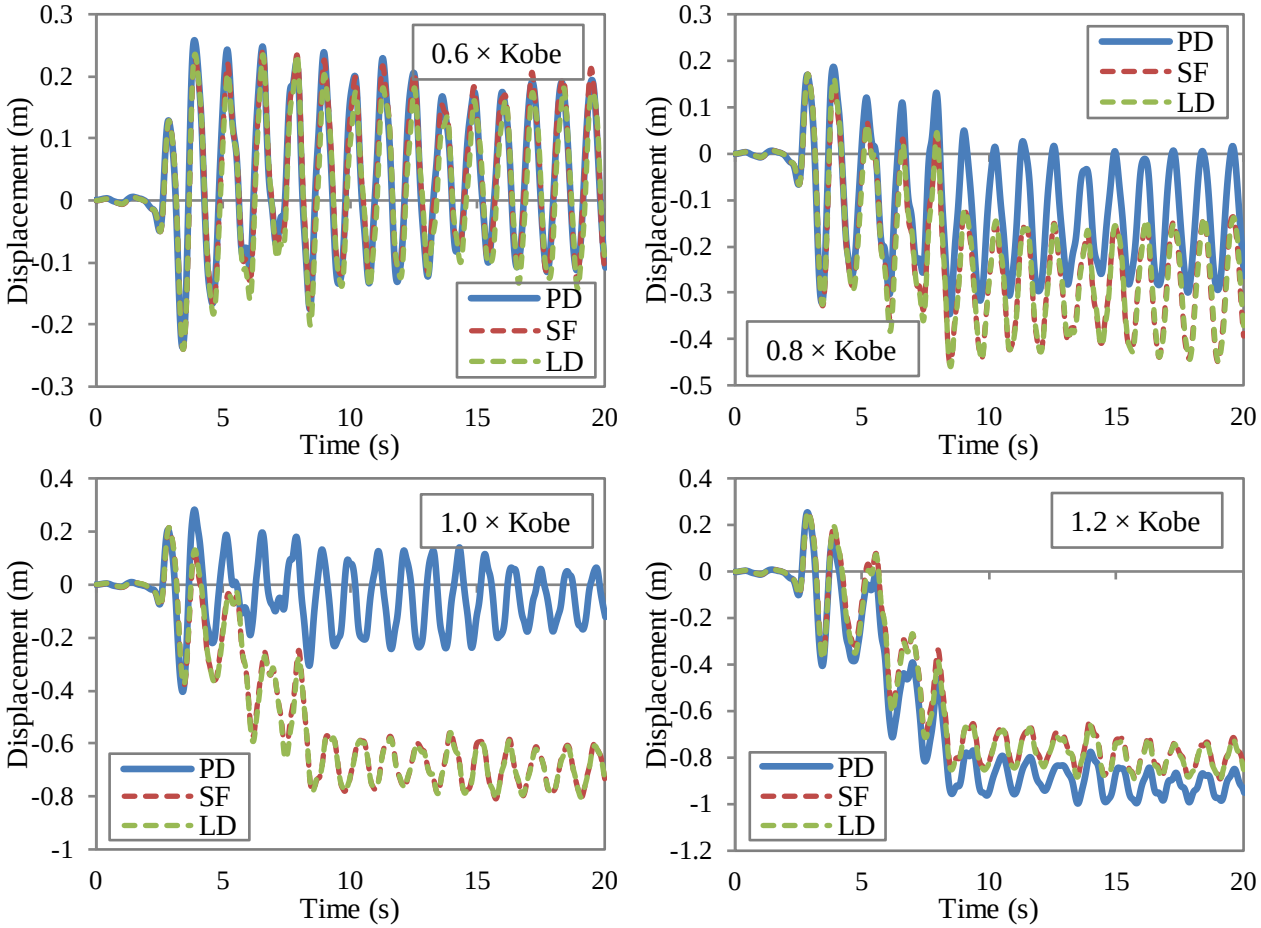

Fig. 8 – Roof displacement response of the four-story frame with various geometric nonlinearities

Since both ASCE/SEI 7-16 and ASCE/SEI 41-17 are design standards with the purpose of limiting damages in structures during major earthquakes, only slight material nonlinearity is expected in the analysis of the designed models. Therefore, any formulation of geometric nonlinearity is appropriate for use in these standards as long as users 'turn on' geometric nonlinearity in the analysis. However, if the analysis requires significant coupling between geometric and material nonlinearities, such as in the case of analyzing structural collapse or near-collapse, the applicability of software packages that implement *P*-Δ stiffness warrants further study.

7. References

[1] ASCE/SEI 7-16 (2016): *Minimum Design Loads for Buildings and Other Structures*. American Society of Civil Engineers, Reston, VA, USA.

[2] ASCE/SEI 41-17 (2017): *Seismic Evaluation and Retrofit of Existing Buildings*. American Society of Civil Engineers, Reston, VA, USA.

[3] Timoshenko SP, Gere JM (1961): *Theory of Elastic Stability*. McGraw Hill, 2nd Edition, NY, USA.

[4] Bazant ZP, Cedolin L (2003): *Stability of Structures*. Dover Publication, NY, USA.

[5] Powell GH (2010): *Modeling for Structural Analysis: Behavior and Basics*. Computers and Structures, CA, USA.

[6] Wilson E (2010): *Static and Dynamic Analysis of Structures: A Physical Approach with Emphasis on Earthquake Engineering*. Computer and Structures, 4th Edition, CA, USA.

